A CFD-based numerical model for predicting the slump and slump flow of fresh concrete from a rheological perspective

Cai, Yuxin; Liu, Qing feng; Chen, Mengzhu; Xiong, Qing Xiang; Šavija, Branko

DOI
10.1016/j.conbuildmat.2024.138501

Publication date
2025

Document Version
Final published version

Published in
Construction and Building Materials

Construction and Building Materials 458 (2025) 138501

Contents lists available at ScienceDirect

Construction and Building Materials

journal homepage: www.elsevier.com/locate/conbuildmat

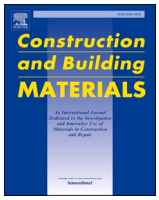

A CFD-based numerical model for predicting the slump and slump flow of fresh concrete from a rheological perspective

Yuxin Cai [a], Qing-feng Liu [a,b,c,*], Mengzhu Chen [d], Qing Xiang Xiong [a], Branko Šavija [e]

[a] State Key Laboratory of Ocean Engineering, School of Ocean and Civil Engineering, Shanghai Jiao Tong University, Shanghai, China
[b] State Key Laboratory of Subtropical Building and Urban Science, South China University of Technology, Guangzhou, China
[c] Shanghai Key Laboratory for Digital Maintenance of Buildings and Infrastructure, Shanghai, China
[d] School of Materials Science and Engineering, Sun Yat-sen University, Guangzhou, China
[e] Microlab, Faculty of Civil Engineering and Geosciences, Delft University of Technology, Delft, the Netherlands

ARTICLE INFO

Keywords:
Flowability
Rheology
Slump test
CFD
Numerical model

ABSTRACT

Herein, a three-dimensional numerical model based on computational fluid dynamics (CFD) for fresh concrete is developed to predict the slump and slump flow. Fresh concrete is considered as a non-Newtonian fluid, and its rheological behaviour is characterised by the Bingham and Herschel-Bulkley (H-B) models, respectively. Experiments are also conducted to validate the reliability and accuracy of this model. Through parametric investigations, the influence mechanisms of relevant factors on the flow characteristics of fresh concrete are analysed and discussed. The results show that the model predictions agree well with the experimental results. The predicted results obtained using the H-B rheological model are more accurate compared to the Bingham model, with average relative errors of 1.73 %, 2.03 % and 3.95 % for slump, slump flow and T_{500}, respectively. The flowability of fresh concrete is negatively correlated with power index, yield stress and consistency, while it is positively correlated with density. Grey relational analysis indicates that density has the greatest effect on the results of slump and slump flow, followed by yield stress and consistency, and finally the power index. The CFD-based numerical model presented in this study provides an important approach for better understanding the flow behaviour of fresh concrete from a rheological perspective.

1. Introduction

Concrete is extensively used in civil engineering, as an affordable building material made from widely available raw materials. After mixing the constituent materials and before hardening, concrete is in a liquid-like state and is referred to as fresh concrete. In practical applications, concrete mixtures need to be poured into moulds or formworks during the fresh stage to form finished products and components with specific shapes. At this stage, fresh concrete should have sufficient flowability to facilitate its transportation, pumping and casting. Flowability refers to the ability of a concrete mixture to flow and uniformly fill the moulds or formworks under its own weight or mechanical vibration. The flow properties have a significant impact on the workability of concrete during the fresh stage, as well as the mechanical strength and durability after setting and hardening [1]. Insufficient flowability makes it difficult to pour and fill the formwork evenly, leading to construction defects such as cavities, honeycombing or exposed reinforcing bars, which will affect the long-term performance of reinforced concrete [2,3]. If the flowability is too high, although it makes construction easier, it may easily lead to stability issues in the concrete mixture causing segregation and affecting the quality of the hardened concrete [4–7].

Fresh concrete is usually regarded as a non-Newtonian fluid, and it only flows and deforms when the shear stress overcomes the yield stress. In most cases, the Bingham model is commonly used to describe the rheological characteristics of fresh concrete [8,9]. However, various mineral and chemical admixtures are often added to improve the performance of modern concretes, which makes the concrete mixture system complex. Some studies [10–13] have found that the shear rate-shear stress curve of concrete mixtures may deviate from the linear relationship with increasing shear rate, exhibiting shear thickening or shear thinning behaviour. Shear thickening refers to the phenomenon where the apparent viscosity gradually increases with increasing shear rate. On the contrary, shear thinning refers to the phenomenon where the apparent viscosity gradually decreases with increasing shear rate. Shear

* Corresponding author at: State Key Laboratory of Ocean Engineering, School of Ocean and Civil Engineering, Shanghai Jiao Tong University, Shanghai, China.
E-mail address: liuqf@sjtu.edu.cn (Q.-f. Liu).

https://doi.org/10.1016/j.conbuildmat.2024.138501
Received 21 November 2023; Received in revised form 3 September 2024; Accepted 24 September 2024
Available online 19 December 2024

thickening behaviour not only causes poor flowability of fresh concrete, but also easily leads to difficulties in pumping and casting during construction [14,15]. Although shear thinning behaviour can improve the flow and deformation abilities of fresh concrete, it tends to cause the segregation, settlement and bleeding [16,17]. In such cases, the Herschel-Bulkley (H-B) model can better characterise the nonlinear rheological behaviour [18]. Wallevik et al. [19] pointed out that the rheological properties of most normal concrete conformed to the Bingham model. In contrast, high-fluidity concrete and self-compacting concrete often exhibited nonlinear rheological characteristics, making the H-B model a more appropriate characterization for their rheological properties. Yahia and Khayat [20] found that, in rheological tests, the yield stresses determined by the H-B model for cement-based materials exhibiting shear thickening were larger, and for those exhibiting shear thinning were smaller, compared to those determined by the Bingham model. According to the findings of Vance et al. [21], in comparison to the value at the stress plateau, the Bingham and H-B rheological models might overestimate and underestimate the apparent yield stress of a given cementitious suspension, respectively. However, when rheological evaluations were extended to much lower shear rates, the yield stress estimated by the H-B model was found to be comparable to the true apparent yield stress observed at the shear stress asymptote.

Currently, slump test is the most frequently used experimental method for evaluating the flow performance of fresh concrete in laboratories and construction sites. However, the design of mix proportions and the properties of raw materials are variable in different working conditions, and even a small change can have a noticeable effect on the flowability of concrete mixtures [22,23]. At this point, a large number of repeated experiments are needed to determine the variation law of the flow behaviour of fresh concrete. However, it not only consumes a lot of manpower and material resources, but also faces challenges in fundamentally explaining the changing characteristics of flow properties. Additionally, the control of rheological parameters and experimental conditions is a tricky problem when researchers attempt to investigate the influence mechanism of a specific factor.

With the rapid development of computer technologies and numerical algorithms, numerical simulation methods are becoming increasingly important in the research field of cement and concrete materials [24–29]. By means of numerical modelling, it is not only possible to efficiently conduct many numerical experiments and minimise the waste of raw materials, but modelling can also help to optimise the mix proportions and achieve suitable flowability. Computational fluid dynamics (CFD) is an interdisciplinary field that lies between mathematics, fluid mechanics and computer science. It solves the governing equations of fluid mechanics through computer technologies and numerical methods to simulate the flow characteristics of fluids [30–33]. The CFD method has the advantage of helping researchers to investigate the flow and deformation phenomena of fluids under a rheological perspective, which can provide important theoretical guidance and technical support for experimental studies on the flowability of fresh concrete. For example, Vasilic et al. [34] simulated the motion process of fresh concrete around steel bars by employing CFD. Sassi et al. [35] adopted a CFD-based model to investigate the flowability of fresh concrete in the L-box test apparatus. Choi et al. [36] explored the potential of using a CFD-based model to analyse the flow behaviour of fresh concrete during the pumping process. Based on CFD technology, Comminal et al. [37] investigated the effects of printing speed and nozzle height on the geometric shape of 3D printed concrete. However, most of these studies overlook the role of nonlinear rheological characteristics on the flow properties of fresh concrete, and the parametric investigations on flowability and the quantitative evaluation of the contribution degree of relevant influencing factors are not systematic enough. Moreover, previous studies lack in-depth discussion on the distribution profile of velocity for fresh concrete during the flow process, particularly ignoring its impact on flow behaviour in the early stage of slump testing.

Herein, a CFD-based numerical model is developed to predict the slump and slump flow of fresh concrete, and the linear and nonlinear rheological characteristics are described using the Bingham and H-B models, respectively. Furthermore, experiments are also conducted to validate the accuracy of model predictions. Based on this model, the effects of power index, yield stress, consistency and density on the flowability of fresh concrete are systematically analysed and discussed, and the contribution degree of these influencing factors is ranked through grey relational analysis. The findings of this study can reveal the underlying mechanism of the flow behaviour of fresh concrete from a fundamental point of view.

2. Experimental program

2.1. Materials and mixtures

The binder materials used in the experiment to prepare the concrete mixture included P.O 42.5 R ordinary Portland cement (OPC), fly ash, slag and silica fume. The basic properties of OPC were measured according to the Chinese standard GB/T 1346-2011 [38], as shown in Table 1. The densities of OPC, fly ash, slag and silica fume were 3020 kg/m^3, 2350 kg/m^3, 2910 kg/m^3 and 2200 kg/m^3, respectively, and their specific surface areas were 340 m^2/kg, 390 m^2/kg, 420 m^2/kg and 22,205 m^2/kg, respectively. The chemical compositions of binder materials were tested using X-ray fluorescence, as presented in Table 2.

River sand with a density of 2690 kg/m^3, a clay content of 1.8 % and a fineness modulus of 2.9 was used as the fine aggregate. Limestone gravel with a particle size of 5−20 mm, a density of 2670 kg/m^3 and a clay content of 0.6 % was used as the coarse aggregate. In addition, a high-performance polycarboxylate-based superplasticizer was used to adjust the workability of concrete mixtures. The specific gravity, solid content and water reduction rate of the superplasticizer were 1.09, 42 % and 40 %, respectively.

In the mix proportion design, the water-to-binder ratio (w/b) was fixed at 0.38, the total amount of binder materials was fixed at 500 kg/m^3, and the dosage of superplasticizer was 0.7 % by mass of the amount of binder materials. Previous studies [39–41] have shown that the addition of silica fume could obviously increase the yield stress and viscosity of mixtures, as well as reduce the flowability of fresh concrete, due to its extremely large specific surface area. Therefore, four groups of concrete mixtures with different rheological parameters and flow properties were designed in the experiment by varying the dosage of silica fume. The concrete mix proportions are shown in Table 3. The apparent densities of these four groups of concrete mixtures were tested according to the Chinese standard GB/T 50080-2016 [42], with an accuracy of 5 kg/m^3. The results were 2405 kg/m^3, 2390 kg/m^3, 2395 kg/m^3 and 2385 kg/m^3, respectively.

2.2. Slump test

The apparatus for the slump test is made up of a bucket, a feed hopper, a tamping rod, a vertical ruler and a base plate, as displayed in Fig. 1(a). The standard slump bucket mould is in the shape of the frustum of a cone with a top diameter of 100 mm, a bottom diameter of 200 mm and a height of 300 mm [43]. Prior to the slump test, the inner wall of the bucket and the base plate were pre-wetted with water. During the test, the concrete mixture sample was placed and compacted by tamping with a rod in the slump bucket mould. Afterwards, the mould

Table 1
Basic properties of OPC.

Cement	Water requirement of normal consistency (%)	Setting time (min)		Soundness
		Initial setting	Final setting	
P.O 42.5 R	28.4	180	240	Qualified

Table 2
Chemical compositions of binder materials (wt%).

Binders	CaO	SiO_2	Al_2O_3	MgO	Fe_2O_3	SO_3	Loss on ignition
OPC	58.99	22.02	6.19	2.53	2.65	2.67	3.08
Fly ash	7.61	49.93	25.75	1.37	9.73	0.12	1.53
Slag	39.00	32.70	14.03	8.99	0.50	0.20	0.78
Silica fume	0.76	87.42	0.29	2.49	1.75	0.48	3.30

was raised, and the sample was allowed to subside and spread under the action of gravity. After the concrete stopped flowing, the vertical distance between the highest position of the collapsed mixture and the height of the mould (300 mm) was measured as the slump. In the meantime, two diameters of the mixture were measured using a steel ruler in approximately orthogonal directions, and the average of the two was recorded as the slump flow (see Fig. 1(b)). Note that the time taken for the mixture to spread to a diameter of 500 mm (T_{500}) was also measured in the experiment to further validate the model.

In this study, in order to obtain more accurate measurement results, the slump, slump flow and T_{500} values of each group of concrete were determined by the average of three times of test results, with a relative error of less than 10 % for these three results. The slump, slump flow and T_{500} results were accurate to 1 mm, 1 mm and 0.01 s, respectively. The experimental results of the slump test are summarised in Table 4. It can be seen that both the slump and slump flow tend to decrease as the dosage of silica fume increases, while the T_{500} value tends to increase. These are associated with the changes in rheological parameters of concrete mixtures, which will be discussed in detail later in this study.

2.3. Rheological test

The rheological parameters of concrete mixtures were tested using an ICAR rheometer, and the vane geometry was a four-bladed shape with a height and diameter of 127 mm. During the flow curve test, the rotational speed was initially increased to 0.50 rps and held for about 20 s (pre-shear phase) to ensure the disruption of the internal structure of concrete mixtures and eliminate the influence of thixotropy on measurement results. Then, the rotational speed was gradually reduced from 0.50 rps to 0.05 rps to obtain the descending curve. The number of test points was 7, with each point lasting for 5 s. After that, the rheological parameters of concrete mixtures were calculated by fitting the descending curve based on both the Bingham model and the H-B model, as expressed in Eqs. (1) and (2), respectively.

$$\tau = \tau_0 + \eta_p \dot{\gamma} \tag{1}$$

$$\tau = \tau_0 + K\dot{\gamma}^n \tag{2}$$

where τ is the shear stress, $\dot{\gamma}$ is the shear rate, τ_0 is the yield stress, η_p is the plastic viscosity, K is the consistency, and n is the power index that reflects the degree of shear thinning or thickening. When $n < 1$, the material exhibits shear thinning behaviour; when $n > 1$, it exhibits shear thickening behaviour; and when $n = 1$, the material is a Bingham fluid.

Note that the flow curve reflects the relationship between the raw measurements of torque and rotational speed. The connection between torque and rotational speed for Bingham and H-B fluids can be repre-

Table 4
Experimental results of the slump test.

Group	Slump (mm)	Slump flow (mm)	T_{500} (s)
1	228	665	2.70
2	220	618	3.08
3	217	597	3.31
4	211	568	3.68

Table 3
Mix proportions of concrete (kg/m^3).

Group	w/b	Water	OPC	Fly ash	Slag	Silica fume	Sand	Gravel	Superplasticizer
1	0.38	190.0	350.0	75.0	75.0	–	765.0	935.0	3.5
2	0.38	190.0	350.0	67.5	67.5	15.0	765.0	935.0	3.5
3	0.38	190.0	350.0	60.0	60.0	30.0	765.0	935.0	3.5
4	0.38	190.0	350.0	52.5	52.5	45.0	765.0	935.0	3.5

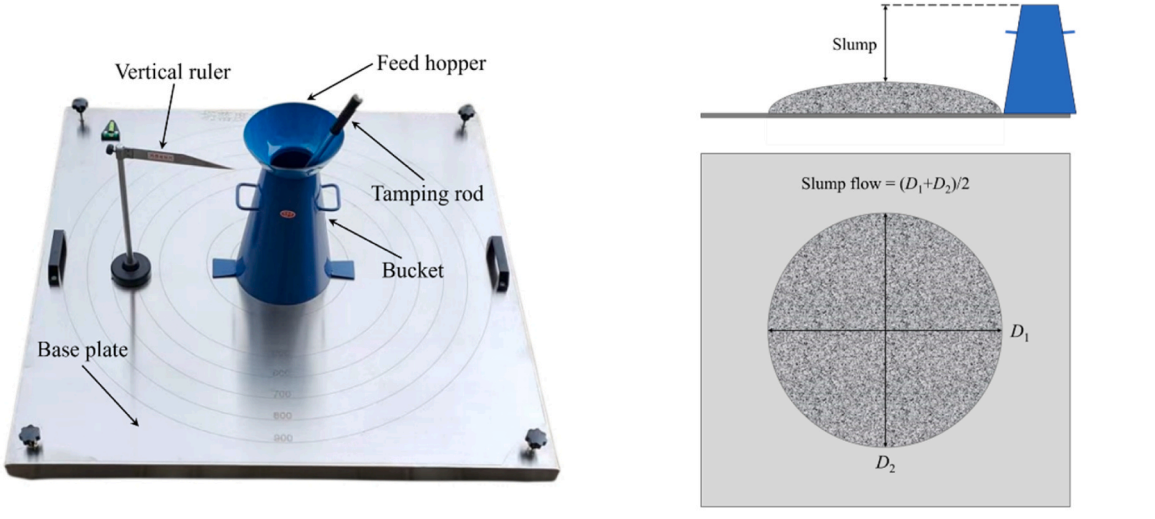

Fig. 1. Details of the slump test.

sented by Eqs. (3) and (4), respectively.

$$T = G_B + H_B N \tag{3}$$

$$T = G_{H-B} + H_{H-B} N^J \tag{4}$$

where T is the torque, N is the rotational speed, G_B and H_B are determined from the torque-rotational speed relationship of the Bingham fluid, which are related to yield stress and plastic viscosity, respectively, and $G_{H\text{-}B}$, $H_{H\text{-}B}$ and J are determined from the torque-rotational speed relationship of the H-B fluid, which are related to yield stress, consistency and power index, respectively.

For the Bingham fluid, the relationships of yield stress and plastic viscosity with respect to G_B and H_B are expressed in Eqs. (5) and (6), respectively.

$$\tau_0 = \frac{G_B}{4\pi h}\left(\frac{1}{R_i^2} - \frac{1}{R_o^2}\right)\frac{1}{\ln(R_o/R_i)} \tag{5}$$

$$\eta_p = \frac{H_B}{8\pi^2 h}\left(\frac{1}{R_i^2} - \frac{1}{R_o^2}\right) \tag{6}$$

For the H-B fluid, the relationships of yield stress, consistency and power index with respect to $G_{H\text{-}B}$, $H_{H\text{-}B}$ and J are expressed in Eqs. (7)–(9), respectively.

$$\tau_0 = \frac{G_{H-B}}{4\pi h}\left(\frac{1}{R_i^2} - \frac{1}{R_o^2}\right)\frac{1}{\ln(R_o/R_i)} \tag{7}$$

$$K = \frac{H_{H-B}}{2^{2n+1}\pi^{n+1}h}n^n\left(\frac{1}{R_i^{2/n}} - \frac{1}{R_o^{2/n}}\right)^n \tag{8}$$

$$n = J \tag{9}$$

where h is the height of the cylinder, R_i is the radius of the inner cylinder, and R_o is the radius of the outer cylinder.

To minimize measurement errors, the final values of rheological parameters of each group of concrete were determined by the average of three times of test results, as shown in Table 5. As can be seen from Table 5, the yield stress and plastic viscosity obtained based on the Bingham rheological model increase with increasing silica fume dosage, which is consistent with the literature [39–41]. As for the yield stress and consistency obtained based on the H-B rheological model, they also exhibit an increasing trend with increasing silica fume dosage. Furthermore, the shear thinning behaviour of concrete mixtures gradually weakens (a larger power index) with increasing silica fume dosage, which demonstrates that the addition of silica fume can mitigate the shear thinning phenomenon to a certain extent in this study.

3. Numerical modelling

3.1. Theoretical method

In this study, the numerical modelling of the slump test is performed based on CFD. The workflow of numerical modelling of fluid flow by employing the CFD method is illustrated Fig. 2. The basic idea behind CFD involves replacing the originally continuous physical field in the temporal and spatial domains with a collection of variable values at a series of discrete points. On the basis of the fluid governing equations, a system of algebraic equations is established to reflect the relationships among the field variables at these discrete points, and the algebraic equations are then solved to derive the approximate values of these field variables.

Fluid flow obeys the conservation laws of mass, momentum and energy, and the governing equations are the mathematical descriptions of them. The mass conservation equation, also known as the continuity equation, can be denoted by Eq. (10).

$$\frac{\partial \rho}{\partial t} + \frac{\partial(\rho u)}{\partial x} + \frac{\partial(\rho v)}{\partial y} + \frac{\partial(\rho w)}{\partial z} = 0 \tag{10}$$

where ρ is the fluid density, t is the time, and u, v and w are the fluid velocity components in the x, y and z directions, respectively.

For any given physical quantity $\vec{a}$, its divergence can be expressed as:

$$\nabla \cdot \vec{a} = \frac{\partial a_x}{\partial x} + \frac{\partial a_y}{\partial y} + \frac{\partial a_z}{\partial z} \tag{11}$$

Therefore, Eq. (10) can be transformed into:

$$\frac{\partial \rho}{\partial t} + \nabla \cdot (\rho \vec{v}) = 0 \tag{12}$$

where $\vec{v}$ represents the velocity vector.

If the fluid is incompressible, the fluid density is a constant and Eq. (10) can be simplified as:

$$\frac{\partial u}{\partial x} + \frac{\partial v}{\partial y} + \frac{\partial w}{\partial z} = 0 \tag{13}$$

The law of momentum conservation is an application of Newton's second law in fluid dynamics. Fresh concrete is generally considered as an incompressible viscous fluid, and its momentum conservation equation is described by the Navier-Stokes equation, as follows:

$$\rho \frac{D\vec{v}}{Dt} = -\nabla p + \mu \nabla^2 \vec{v} + \vec{F} \tag{14}$$

where $\frac{D\vec{v}}{Dt}$ is the material derivative, p is the pressure, μ is the dynamic

Table 5
Rheological parameters of fresh concrete.

Group	Bingham model		H-B model		
	Yield stress (Pa)	Plastic viscosity (Pa·s)	Yield stress (Pa)	Consistency (Pa·s^n)	Power index
1	271.3	35.8	260.1	48.7	0.77
2	302.7	38.3	291.7	51.0	0.83
3	328.6	40.1	312.3	53.2	0.86
4	350.8	42.3	332.2	55.1	0.91

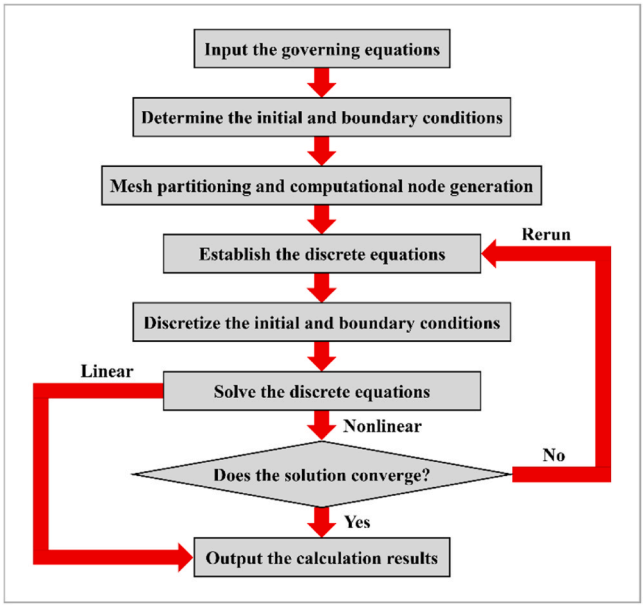

Fig. 2. The workflow diagram of CFD.

viscosity, and $\vec{F}$ is the volume force.

The material derivative of any physical quantity $\vec{a}$ is defined as:

$$\frac{D\vec{a}}{Dt} = \frac{\partial \vec{a}}{\partial t} + (\vec{v}\cdot\nabla)\vec{a} \tag{15}$$

As a result, Eq. (14) is further expressed as:

$$\underbrace{\rho\left[\frac{\partial \vec{v}}{\partial t} + (\vec{v}\cdot\nabla)\vec{v}\right]}_{1} = \underbrace{-\nabla p}_{2} + \underbrace{\mu\nabla^2\vec{v}}_{3} + \underbrace{\vec{F}}_{4} \tag{16}$$

where the first, second, third and fourth terms represent inertial force, pressure, viscous force and external force acting on the fluid, respectively.

If the volume force is only gravity and the z-axis is oriented vertically upwards, it can be expressed as:

$$\begin{cases} F_x = 0 \\ F_y = 0 \\ F_z = -\rho g \end{cases} \tag{17}$$

where F_x, F_y and F_z represent the volume forces in the x, y and z directions, respectively, and g is the gravitational acceleration.

The law of energy conservation is an application of the first law of thermodynamics in fluid dynamics, and it is a fundamental law that must be satisfied for the flow system with heat exchange. The expression is as follows:

$$\frac{\partial(\rho T)}{\partial t} + \nabla\cdot(\rho\vec{v}T) = \nabla\cdot\left(\frac{k}{c_p}\mathrm{grad}T\right) + S_T \tag{18}$$

where T is the thermodynamic temperature, k is the heat transfer coefficient, c_p is the specific heat capacity, and S_T is the viscous dissipation term.

Note that fresh concrete is an incompressible viscous fluid, and the heat exchange during the flow process is very small or even negligible. Consequently, the energy conservation equation is not considered in this study.

3.2. Model establishment

During the modelling process, a space of 1000 mm × 1000 mm × 500 mm was taken as the workspace. The frustum of a cone with a top diameter of 100 mm, a bottom diameter of 200 mm and a height of 300 mm in the centre of the workspace represented the initial state of fresh concrete, while the rest of the workspace represented air at standard atmospheric pressure, as shown in Fig. 3(a). Earlier studies [44,45] have shown that the slump and slump flow were almost independent of the shape of the mould, and the use of the mould merely confined the initial position of the concrete. Hence, the model did not consider the shear stress acting on the concrete by the mould wall. Moreover, considering that the base plate needed to be pre-wetted prior to the slump test, this would result in a thin layer of water film formed between the concrete mixture and the base plate. At this time, the lateral flow of the concrete mixture primarily caused the shear behaviour with the water film, and thus there was almost no slip behaviour between the concrete mixture and the base plate. As a result, the base plate of the workspace was regarded as a no-slip boundary condition with the concrete mixture.

Before the slump test, the velocity components of fresh concrete in the x, y and z directions within the region of the frustum of a cone were set as $u = 0$, $v = 0$ and $w = 0$, respectively. The acceleration due to gravity within the workspace was 9.8 m/s^2, and its direction was vertically downwards. The concrete mixture was regarded as an incompressible non-Newtonian fluid in the numerical model, and the time step for numerical calculations was 0.05 s. Additionally, Reynolds number (Re) was a dimensionless parameter used to characterise the type of fluid, which could be calculated by Eq. (19). The critical value of Re when the fluid type changed was not fixed. It was generally considered that when Re < 2000, the flow of fluid was laminar; when Re > 4000, the flow of fluid was turbulent; and when Re was between these two values, the flow of fluid was in a transitional state [46,47]. Considering that the movement velocity of concrete mixtures during the slump test was relatively low, Re was a small value. Therefore, the flow of fresh concrete was considered as laminar in the numerical model.

$$\mathrm{Re} = \frac{\rho V L}{\eta} \tag{19}$$

where V is the fluid velocity, η is the fluid viscosity, and L is the characteristic length.

It should be noted that the constitutive equations for the Bingham and H-B rheological models are piecewise functions, as shown in Eqs. (20) and (21). There may exist a non-yielding region in flowing concrete, where the shear rate is very small, the shear stress is lower than the yield stress, and the apparent viscosity theoretically tends to infinity. This often leads to instability and non-convergence in numerical calculations.

$$\begin{cases} \tau = \tau_0 + \eta_p\dot{\gamma}, |\tau| > \tau_0 \\ \dot{\gamma} = 0, |\tau| \le \tau_0 \end{cases} \tag{20}$$

$$\begin{cases} \tau = \tau_0 + K\dot{\gamma}^n, |\tau| > \tau_0 \\ \dot{\gamma} = 0, |\tau| \le \tau_0 \end{cases} \tag{21}$$

To address this issue, the rheological models were modified in this study by drawing on Ref. [48], as follows:

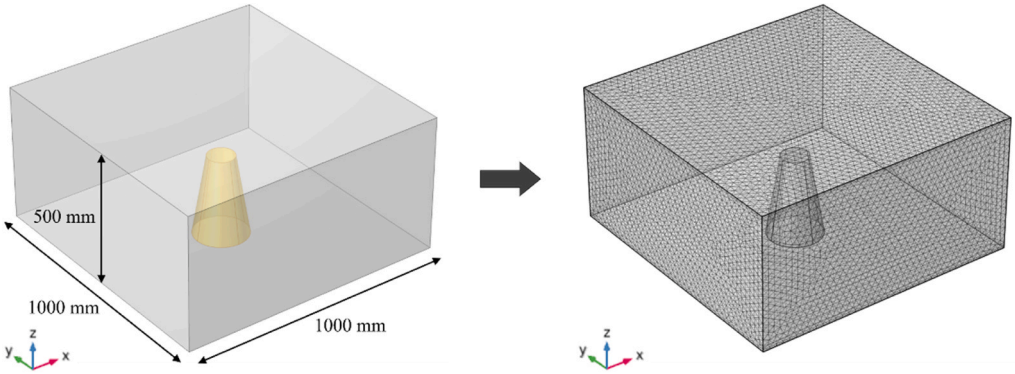

Fig. 3. Geometric model of the slump test.

$$\tau = \tau_0[1 - \exp(-m\dot{\gamma})] + \eta_p\dot{\gamma} \quad (22)$$

$$\tau = \tau_0[1 - \exp(-m\dot{\gamma})] + K\dot{\gamma}^n \quad (23)$$

Here, m is a regularization parameter, which can control the increase of stress to avoid discontinuities in rheological model equations. When m tended to be zero, Eq. (23) was equivalent to the power law model equation. While when m tended to be infinity, Eqs. (22) and (23) ideally approached the equations of Bingham and H-B models. Accordingly, a larger value of m could better reduce the errors after modifying the rheological model equations. However, if the value of m was too large, it would significantly increase the computation time and even lead to non-convergence of the solution [49]. Therefore, m was taken as 500 in this study as proposed by Wu et al. [50].

The mesh division for the numerical model of the slump test is shown in Fig. 3(b). It is worth noting that a finer grid could result in a smaller Peclet number, which was beneficial for reducing numerical oscillations to obtain more accurate results [51–53]. However, this was also accompanied by higher computational costs [54–56]. Before the mesh division, sensitivity analysis was conducted to determine the appropriate grid size. It was found that in this model, a minimum grid size of approximately 2.83×10^{-3} m could achieve a good balance between accuracy and computational time. At this time, the number of grids was 4.91×10^5. In addition, the grid shape was predominantly free tetrahedral, as this type of grids offered the best adaptability to geometric models and efficiency for numerical calculations [57,58].

3.3. Model validation

In this section, the accuracy of model predictions of slump, slump flow and T_{500} was validated through the experimental results presented in Section 2.2. During the modelling process, the rheological parameters of these four groups of fresh concrete, including the Bingham and H-B rheological models, were set to be consistent with the experimentally measured results (see Table 5). Moreover, the densities of these four groups of fresh concrete were set as 2405 kg/m^3, 2390 kg/m^3, 2395 kg/m^3 and 2385 kg/m^3, which were also measured from experiments. Taking the first group as an example, the profile diagrams of the slump process of concrete mixtures in the numerical models using both Bingham and H-B rheological models are depicted in Fig. 4. From Fig. 4, it can be observed that fresh concrete collapses rapidly under the influence of gravity at the beginning, and then the flow gradually slows down in the later period. Compared to the fresh concrete characterised by the Bingham rheological model, the concrete characterised using the H-B rheological model exhibits faster flow, as evidenced by greater results of slump and slump flow at the same time. This is because the H-B model can capture the nonlinear rheological behaviour, and further discussions will be presented in Section 4.1.

Through many models, it is found that fresh concrete virtually stops flowing after 15.0 s, so the values of slump and slump flow at 15.0 s are

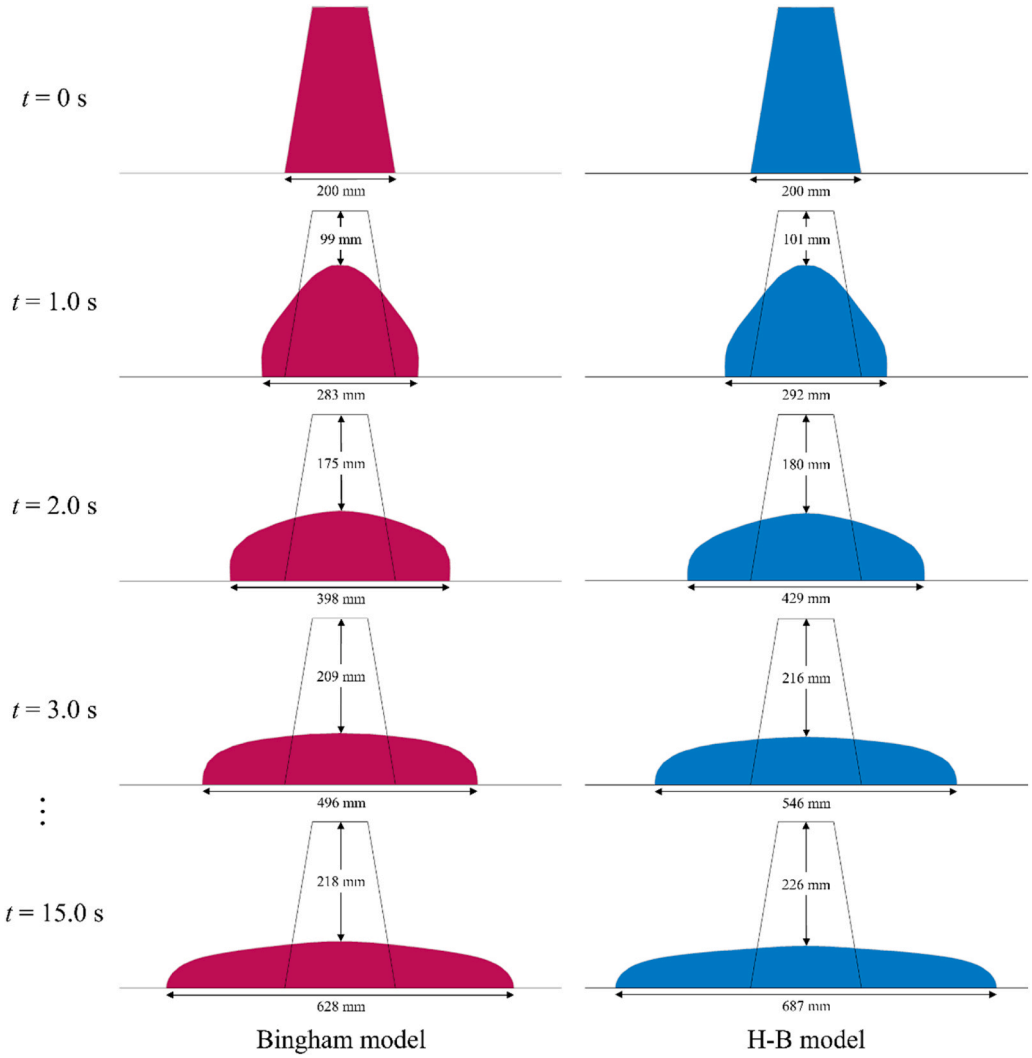

Fig. 4. Profile diagrams of the slump process of fresh concrete (taking the first group as an example).

taken as the final results. The comparison of slump, slump flow and T_{500} between the numerical model predictions and the experimental results is illustrated in Fig. 5. Overall, the model predictions agree well with experiments, indicating that the CFD-based numerical model is applicable and reliable for simulating the slump test. To quantitatively validate the reliability and accuracy of the present model, the errors of model predictions relative to experimental results are calculated by Eqs. (24)–(26) for slump, slump flow and T_{500}, respectively.

$$\delta_s = \left|\frac{s - s^*}{s^*}\right| \times 100\% \tag{24}$$

$$\delta_{sf} = \left|\frac{s_f - {s_f}^*}{{s_f}^*}\right| \times 100\% \tag{25}$$

$$\delta_{T500} = \left|\frac{t_{500} - {t_{500}}^*}{{t_{500}}^*}\right| \times 100\% \tag{26}$$

where δ_s, δ_{sf} and δ_{T500} represent the relative errors between model predictions and experimental results for slump, slump flow and T_{500}, respectively, s, s_f and t_{500} represent the model predictions of slump, slump flow and T_{500}, respectively, and s^*, ${s_f}^*$ and ${t_{500}}^*$ represent the experimental results of slump, slump flow and T_{500}, respectively.

The error analysis results of fresh concrete flowability between the numerical model predictions and the experimental results are presented in Table 6. For fresh concrete characterized by the Bingham rheological model, the numerical model's predicted error for slump ranges from 1.90 % to 4.39 % relative to experimental results. The relative error for slump flow ranges from 2.29 % to 5.56 %, and for T_{500}, it ranges from 2.72 % to 12.96 %. The average relative errors of these three flowability indicators are 3.18 %, 3.74 % and 6.18 %, respectively. While for the fresh concrete characterised by the H-B rheological model, the error of the slump value predicted by the numerical model ranges from 0.88 % to 2.37 % relative to experimental results, the relative error of slump flow ranges from 0.65 % to 3.31 %, and the relative error of T_{500} ranges from 1.85 % to 4.89 %. In comparison to the Bingham model, the predicted results obtained using the H-B model are more accurate. The average relative errors of slump, slump flow and T_{500} based on the H-B model are 1.73 %, 2.03 % and 3.95 %, respectively. This is because the H-B model can properly consider the nonlinear rheological behaviour, thereby obtaining more accurate predicted results. For example, the maximum errors of slump, slump flow and T_{500} for the fresh concrete characterised by the Bingham rheological model all occur in the first group. From Table 5, it is found that the shear thinning behaviour is the most severe at this point. The above analysis confirms the importance of considering shear thinning or shear thickening behaviour when studying the flowability of fresh concrete.

Table 6
Error analysis of fresh concrete flowability between model predictions and experimental results.

Group	Bingham model			H-B model		
	δ_s	δ_{sf}	δ_{T500}	δ_s	δ_{sf}	δ_{T500}
1	4.39 %	5.56 %	12.96 %	0.88 %	3.31 %	1.85 %
2	3.18 %	3.40 %	5.52 %	1.36 %	0.65 %	4.22 %
3	3.23 %	3.69 %	2.72 %	2.30 %	1.17 %	4.83 %
4	1.90 %	2.29 %	3.53 %	2.37 %	2.99 %	4.89 %
Average	3.18 %	3.74 %	6.18 %	1.73 %	2.03 %	3.95 %

4. Parametric investigations

Based on the CFD-based numerical method developed in this study, a series of models can be established to carry out parametric

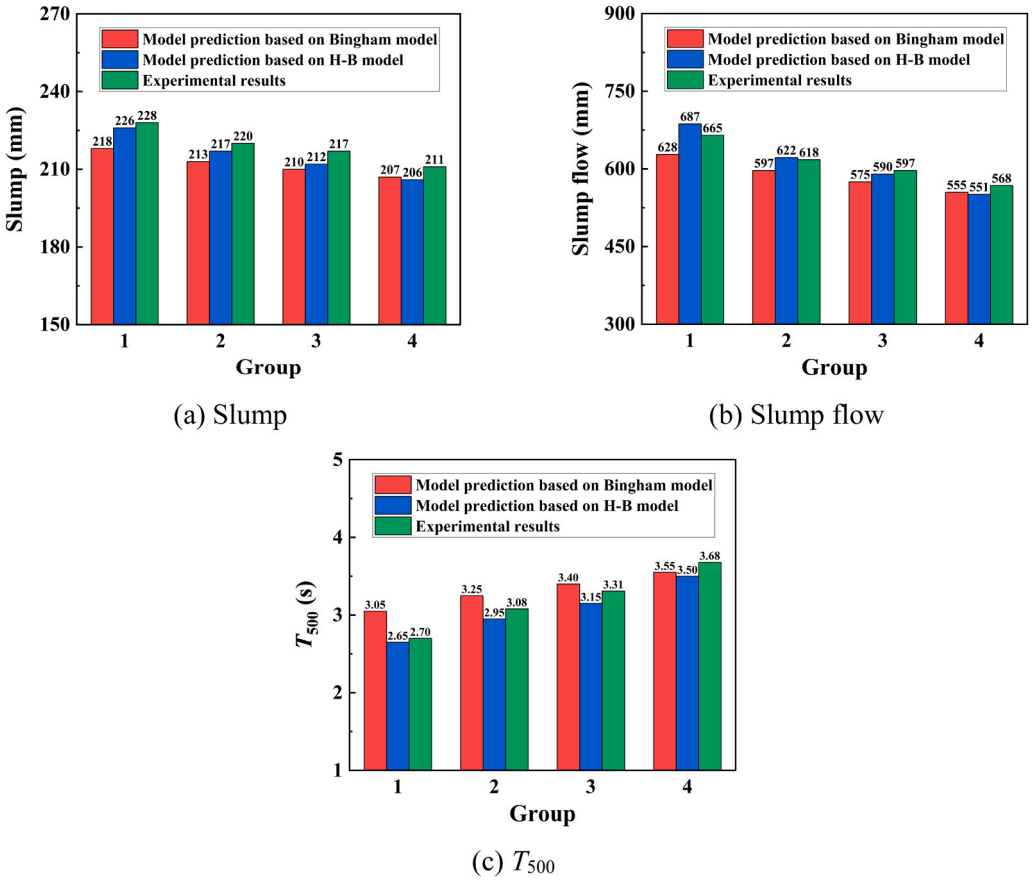

Fig. 5. Comparison of fresh concrete flowability between model predictions and experimental results.

investigations. Compared to experimental studies, numerical simulation methods are not only cost-effective and time-saving but can also facilitate the investigation of the influence mechanism of a single factor on the flow behaviour of fresh concrete. Considering that Section 3.3 shows that the predicted results obtained using the H-B model are closer to actual experimental data compared to the Bingham model, this section will systematically analyse the effects of relevant factors such as power index, yield stress, consistency and density on slump and slump flow on the basis of the H-B model.

4.1. Effect of power index

In the constitutive equation of the H-B model, when the power index is less than 1, the fresh concrete exhibits shear thinning behaviour, while when the power index is greater than 1, it exhibits shear thickening behaviour. The degree of shear thinning or shear thickening behaviour increases as the value of the power index deviates from 1, and the power index value is typically less than 2 for fresh concrete [59,60]. In this section, the yield stress, consistency and density of concrete mixtures were fixed at 300 Pa, 50 Pa·s^n and 2400 kg/m^3, respectively, and the power indexes were set as 0.70, 0.85, 1.00, 1.15 and 1.30 to study the influence of nonlinear rheological characteristics on the flowability of fresh concrete. The developments of slump and slump flow over time for fresh concrete with different power indexes are displayed in Fig. 6. It is found that the slump and slump flow both decrease as the power index increases. The stronger the degree of shear thinning, the higher the flowability, while the stronger the degree of shear thickening, the lower the flowability. The results indicate that shear thinning or shear thickening behaviour needs to be properly considered when modelling of the flow properties of fresh concrete.

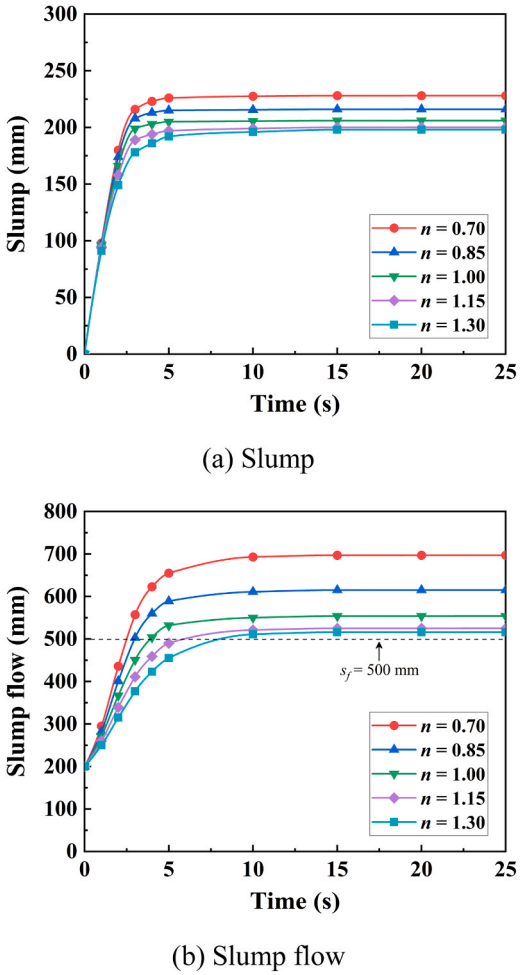

Fig. 6. Effect of power index on slump and slump flow.

It is noticeable to mention that the durations of the changes in slump and slump flow are different. From Fig. 6(a), it can be noticed that the slump rapidly increases within the first 3.0 s, and then gradually stabilises at 5.0 s. Whereas, the slump flow rapidly increases within the first 5.0 s, and then gradually stabilises at 10.0 s (see Fig. 6(b)). Additionally, the slope of the curve of slump flow with time during the period of 0–1.0 s is smaller than that during the period of 1.0–3.0 s. The above results imply that, during the slump test, the vertical flow (change in slump) of fresh concrete occurs very rapidly in the beginning of collapse, while the peak rate of horizontal flow (change in slump flow) lags slightly behind. Compared to the vertical flow, the horizontal flow of fresh concrete ends later.

Fig. 7 shows the velocity profile diagrams of fresh concrete with power indexes of 0.70 and 1.30 in the early stage of slump testing. Regardless of whether fresh concrete exhibits shear thinning or thickening, the peak velocity region is concentrated at the top and the minimum velocity region is concentrated at the bottom in the beginning of the slump test. As the collapse progresses, the region of peak velocity gradually shifts towards the forefront of the fresh concrete flowing in the lateral direction, while the velocity in the central region at the bottom of concrete mixtures is consistently close to zero. In particular, compared to shear thickening concrete, shear thinning concrete exhibits a greater peak flow velocity at the same time point. This provides a good explanation for the phenomena observed in Fig. 6, where the development of slump ends earlier compared to slump flow and shear thinning concrete exhibits higher flowability compared to shear thickening concrete.

4.2. Effect of yield stress

The consistency and density of fresh concrete were set as 50 Pa·s^n and 2400 kg/m^3, respectively. A series of numerical models were developed to analyse the effect of different yield stresses (200 Pa, 250 Pa, 300 Pa, 350 Pa and 400 Pa) on the flowability of fresh concrete exhibiting shear thinning (n = 0.70) or shear thickening (n = 1.30) behaviour. The slump and slump flow results of fresh concrete with different yield stresses are presented in Fig. 8. Both slump and slump flow decrease as the yield stress increases, and the change in yield stress has a greater impact on slump flow in comparison to slump. As the yield stress increases from 200 Pa to 400 Pa, the slump and slump flow of shear thinning concrete decrease by 6.38 % and 17.69 %, respectively, while for shear thickening concrete, the slump and slump flow decrease by 10.90 % and 19.59 %, respectively.

Similar to the findings of this study, Roussel [61] and Sedran and De Larrard [62] also found a negative correlation between the slump and slump flow and the yield stress in their studies, and they established empirical formulas to describe the relationships between them. Furthermore, this study aims to predict the slump and slump flow of fresh concrete from a rheological perspective, and conversely, the magnitude of yield stress can also be roughly estimated based on the flow behaviour exhibited by fresh concrete. For example, Saak et al. [63] estimated the yield stress of concrete mixtures on the basis of slump and slump flow results, and they pointed out that the fundamental relationship between slump and yield stress was independent of the material under study and largely unaffected by the geometric shape of the slump bucket mould.

4.3. Effect of consistency

In this section, the yield stress and density of concrete mixtures were fixed at 300 Pa and 2400 kg/m^3, and the influence of different consistencies of 30 Pa·s^n, 40 Pa·s^n, 50 Pa·s^n, 60 Pa·s^n and 70 Pa·s^n on the flowability of fresh concrete exhibiting shear thinning (n = 0.70) or shear thickening (n = 1.30) behaviour was analysed and discussed. Fig. 9 displays the slump and slump flow results of fresh concrete with

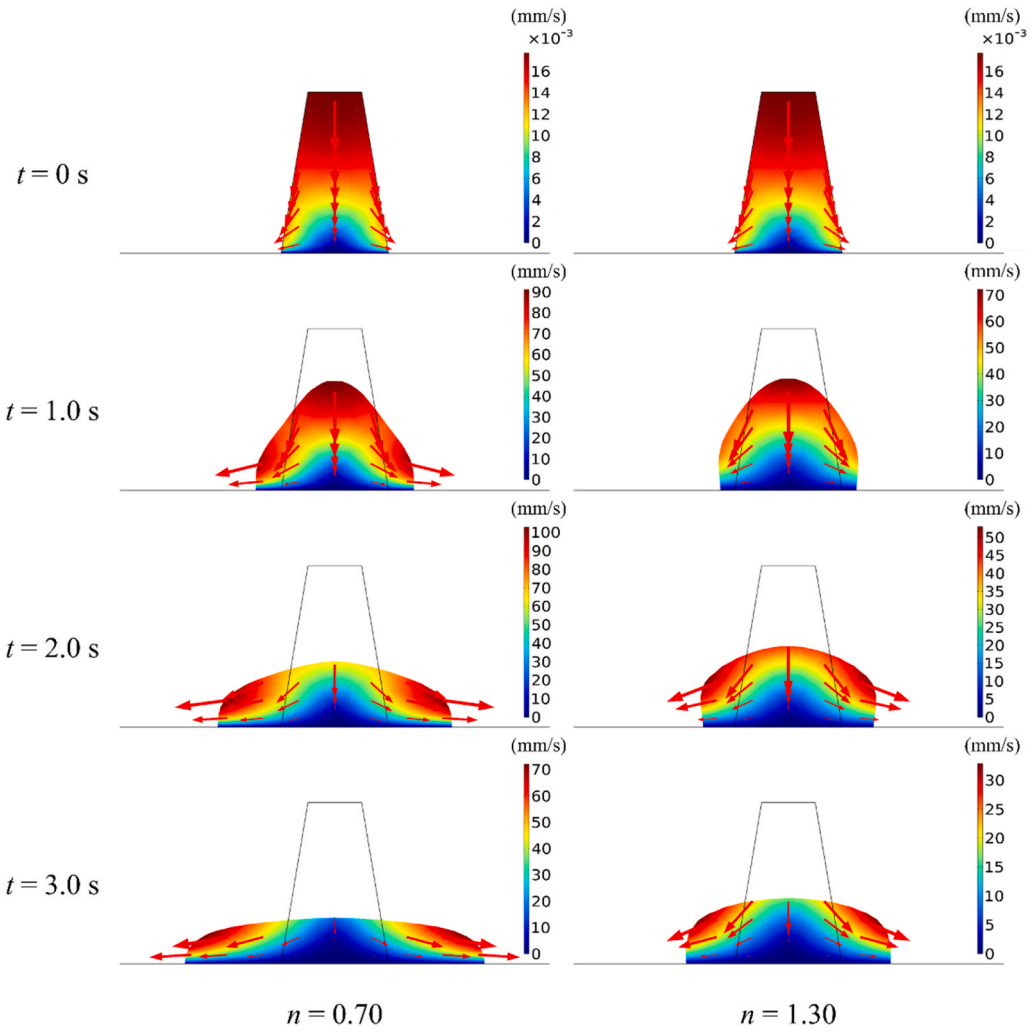

Fig. 7. Velocity profile diagrams of fresh concrete with power indexes of 0.70 and 1.30 in the early stage of slump testing.

different consistencies. It can be observed that both slump and slump flow show a decreasing trend with increasing consistency. In the case of shear thinning concrete with a power index of 0.70, when the consistency increases from 30 Pa·s^n to 70 Pa·s^n, the slump and slump flow decrease by 21 mm and 175 mm, respectively. While in the case of shear thickening concrete with a power index of 1.30, when the consistency increases from 30 Pa·s^n to 70 Pa·s^n, the changes in slump and slump flow are small, decreasing only by 6 mm and 33 mm, respectively. The above results demonstrate that the change in consistency has a greater impact on the flowability of shear thinning concrete compared to shear thickening concrete.

4.4. Effect of density

During the slump test, the flow of fresh concrete occurs under the influence of its own weight. Therefore, it is necessary to study the effect of the density of concrete mixtures on slump and slump flow. In this section, the yield stress of fresh concrete was fixed at 300 Pa and the consistency was fixed at 50 Pa·s^n. A series of numerical models for the fresh concrete with different densities ranging from 1600 kg/m^3 to 2800 kg/m^3 have been established. The slump and slump flow results of fresh concrete with different densities are presented in Fig. 10.

As can be seen from Fig. 10, the flowability of fresh concrete exhibits a highly positive correlation with its density. Both slump and slump flow clearly increase with increasing density, and the growth trend gradually slows down. When the density increases from 1600 kg/m^3 to 2800 kg/m^3, the slump and slump flow of shear thinning concrete increase by 16.34 % and 44.57 %, respectively, while the slump and slump flow of shear thickening concrete increase by 10.93 % and 23.36 %, respectively. In addition, in terms of the magnitude of changes, the increase in density has a greater impact on slump flow compared to slump, and it has a greater impact on the flowability of shear thinning concrete compared to shear thickening concrete. It is noteworthy that in engineering practice, relying solely on gravity is not sufficient for lightweight concrete to achieve good flowability, and it is also required to adjust the rheological parameters of the concrete mixture by adding mineral and chemical admixtures to improve the flowability [64–66].

4.5. Grey relational analysis

Grey relational analysis is a statistical method that determines the degree of correlation between relevant factors based on the degree of similarity or dissimilarity in their development trends [67,68]. In this section, this method is adopted to quantitatively investigate and compare the degree of the influence of relevant factors on the slump and slump flow of fresh concrete. Here, the slump and slump flow are considered as reference sequences, and relevant influencing factors such as power index, yield stress, consistency and density are considered as comparative sequences.

Since the dimensions of each group of data are different, it is inconvenient to directly compare them, and it is also difficult to draw conclusions. Therefore, before conducting the grey relational analysis, it

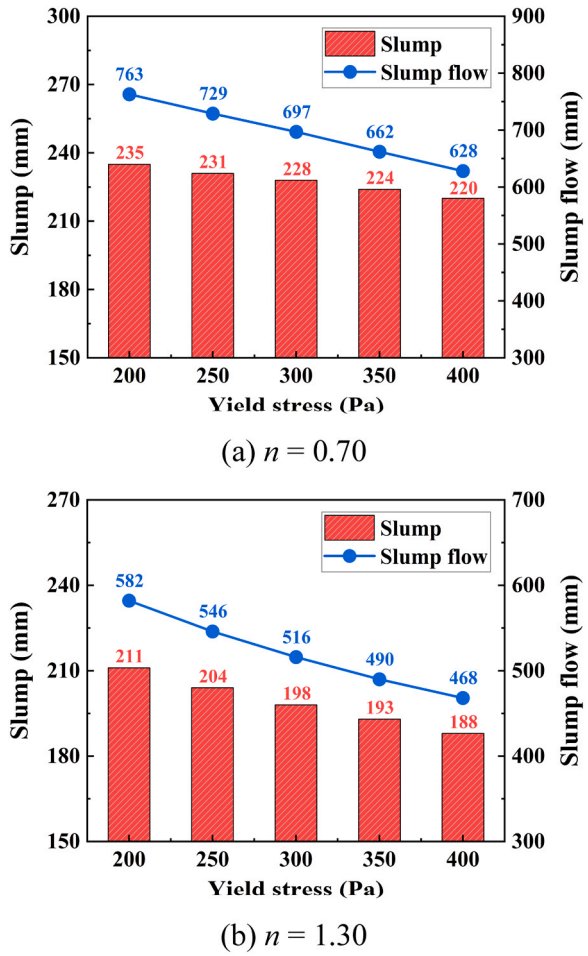

Fig. 8. Effect of yield stress on slump and slump flow.

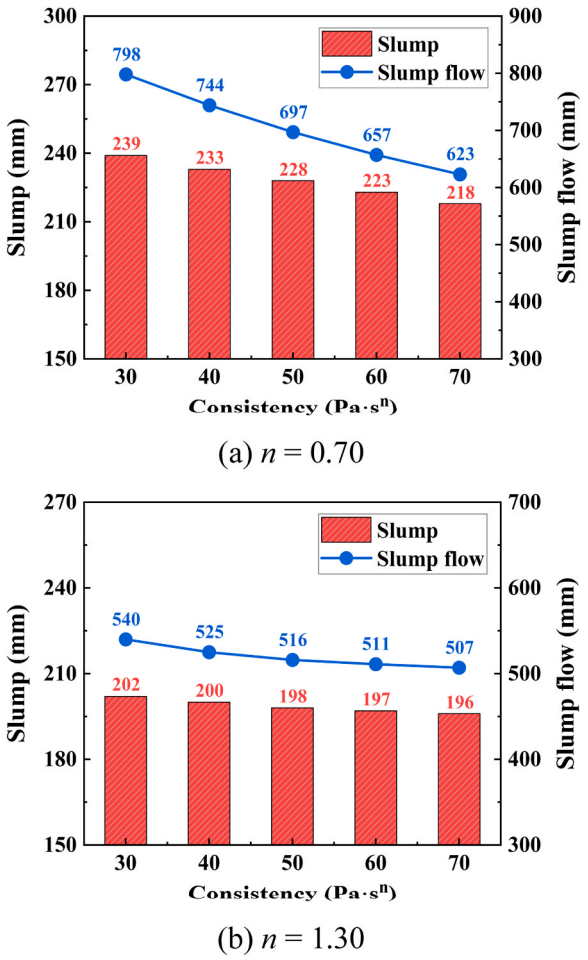

Fig. 9. Effect of consistency on slump and slump flow.

is generally necessary to perform dimensionless processing on the data sequences. In this study, the mean method is used for dimensionless processing, as follows:

$$x_0(k) = \frac{X_0(k)}{\frac{1}{n}\sum_{k=1}^{n} X_0(k)} \tag{27}$$

$$x_i(k) = \frac{X_i(k)}{\frac{1}{n}\sum_{k=1}^{n} X_i(k)} \tag{28}$$

Here, $X_0(k)$ and $X_i(k)$ represent the reference and comparative sequences, and $x_0(k)$ and $x_i(k)$ represent the processed reference and comparative sequences, where $i = 1, 2, 3, \ldots, m$, and $k = 1, 2, 3, \ldots, n$.

After the dimensionless data sequences are prepared, the grey relational coefficients can be calculated using the following equation:

$$\varepsilon_i(k) = \frac{\Delta_{\min} + r\Delta_{\max}}{\Delta_{0i}(k) + r\Delta_{\max}} \tag{29}$$

where r represents the resolution coefficient, which is typically taken as 0.5. The mathematical expressions for $\Delta_{0i}(k)$, $\Delta_{\max}$ and $\Delta_{\min}$ are shown in Eqs. (30)–(32), respectively.

$$\Delta_{0i}(k) = |x_0(k) - x_i(k)| \tag{30}$$

$$\Delta_{\max} = \max_i \max_k |x_0(k) - x_i(k)| \tag{31}$$

$$\Delta_{\min} = \min_i \min_k |x_0(k) - x_i(k)| \tag{32}$$

Considering that the calculated grey relational coefficients are numerous and their values are discrete, the relational coefficients of each group of comparative sequences are averaged to obtain the relational grade, as follows:

$$\gamma_i = \frac{1}{n}\sum_{k=1}^{n} \varepsilon_i(k) \tag{33}$$

where γ_i represents the grey relational grade. A larger value of γ_i indicates a greater influence of this factor on slump and slump flow.

The results of grey relational analysis for slump and slump flow under different influencing factors are given in Table 7. The grey relational grades of power index, yield stress, consistency and density with respect to the slump of fresh concrete are 0.4538, 0.7217, 0.7146 and 0.7740, respectively, and the grey relational grades of these four factors with respect to the slump flow are 0.5012, 0.7066, 0.7032 and 0.7614, respectively. Whether it is for slump or slump flow, the order of relational grades of relevant influencing factors from strong to weak is density, yield stress, consistency and power index. This implies that density has the greatest effect on the slump and slump flow of fresh concrete, followed by yield stress and consistency, and finally the power index. However, it should be noted that although the power index has a smaller effect on the results of slump and slump flow compared to other factors, it significantly affects the flow velocity of the concrete mixture, as indicated by the velocity profile diagrams shown in Fig. 7.

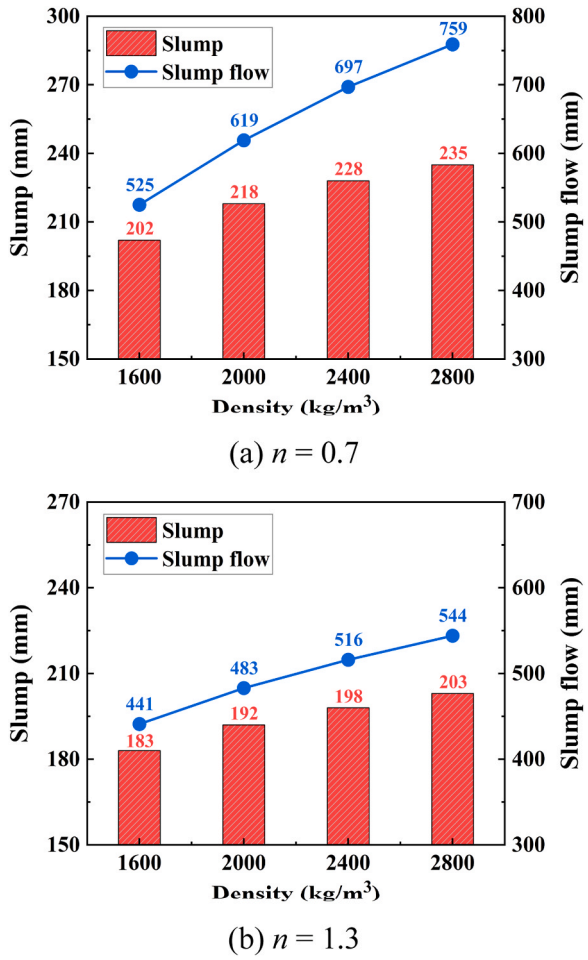

Fig. 10. Effect of density on slump and slump flow.

5. Conclusions

In this study, a CFD-based numerical model has been developed to investigate the flow behaviour of fresh concrete through the slump test, and experiments have been conducted to validate the reliability and accuracy of this model. The influence of relevant factors on the slump and slump flow of fresh concrete has also been systematically discussed. The conclusions can be summarised as follows:

(1) The model predictions agree well with the experimental results. Compared to the Bingham rheological model, the H-B rheological model provides more accurate predictions, with average relative errors of 1.73 %, 2.03 % and 3.95 % for slump, slump flow and T_{500}, respectively. It confirms the importance of considering the nonlinear rheological behaviour in the study of fresh concrete flowability.

(2) During the slump test, the durations of the changes in slump and slump flow are different. In the beginning of concrete flow, the peak velocity region is concentrated at the top. As the collapse progresses, the region of peak velocity gradually shifts towards the forefront of the fresh concrete flowing laterally. Therefore, the change in slump occurs more rapidly in the beginning of flow, and the change in slump flow ends later.

(3) Based on parametric investigations, it is found that the slump and slump flow of fresh concrete are negatively correlated with power index, yield stress and consistency, while positively correlated with density. In particular, the changes in various influencing factors have a greater impact on slump flow than slump. Moreover, the changes in consistency and density have a more significant impact on the flowability of shear thinning concrete than shear thickening concrete.

(4) Grey relational analysis demonstrates that density has the greatest effect on the slump and slump flow of fresh concrete, followed by yield stress and consistency. Compared to the former three influencing factors, although the power index has a smaller effect on the results of slump and slump flow, it significantly affects the flow velocity of the concrete mixture during the slump test.

Table 7
Grey relational analysis for slump and slump flow under different influencing factors.

Group	Slump (mm)	Slump flow (mm)	Power index	Yield stress (Pa)	Consistency (Pa·s^n)	Density (kg/m^3)
1	228	697	0.70	300	50	2400
2	216	615	0.85	300	50	2400
3	206	554	1.00	300	50	2400
4	200	525	1.15	300	50	2400
5	198	516	1.30	300	50	2400
6	235	763	0.70	200	50	2400
7	231	729	0.70	250	50	2400
8	224	662	0.70	350	50	2400
9	220	628	0.70	400	50	2400
10	211	582	1.30	200	50	2400
11	204	546	1.30	250	50	2400
12	193	490	1.30	350	50	2400
13	188	468	1.30	400	50	2400
14	239	798	0.70	300	30	2400
15	233	744	0.70	300	40	2400
16	223	657	0.70	300	60	2400
17	218	623	0.70	300	70	2400
18	202	540	1.30	300	30	2400
19	200	525	1.30	300	40	2400
20	197	511	1.30	300	60	2400
21	196	507	1.30	300	70	2400
22	202	525	0.70	300	50	1600
23	218	619	0.70	300	50	2000
24	235	759	0.70	300	50	2800
25	183	441	1.30	300	50	1600
26	192	483	1.30	300	50	2000
27	203	544	1.30	300	50	2800
Grey relational grade of slump			0.4538	0.7217	0.7146	0.7740
Grey relational grade of slump flow			0.5012	0.7066	0.7032	0.7614

CRediT authorship contribution statement

Qing-feng Liu: Writing – review & editing, Validation, Supervision, Resources, Project administration, Methodology, Funding acquisition. **Yuxin Cai:** Writing – review & editing, Writing – original draft, Visualization, Software, Investigation, Conceptualization. **Qing Xiang Xiong:** Visualization, Validation, Resources, Methodology, Investigation. **Mengzhu Chen:** Validation, Software, Investigation, Formal analysis, Data curation. **Branko Šavija:** Writing – review & editing, Validation, Supervision, Formal analysis, Conceptualization.

Declaration of Competing Interest

The authors declare that they have no known competing financial interests or personal relationships that could have appeared to influence the work reported in this paper.

Data availability

The data that has been used is confidential.

Acknowledgments

This work was financially supported by the National Natural Science Foundation of China (Grant Nos. 52222805 and 52478264), the Natural Science Foundation of Chongqing, China (Grant No. cstb2024nscq-jqX0007), and the Open Foundation of the State Key Laboratory of Subtropical Building and Urban Science (Grant No. 2023KA03).

References

[1] K. Kovler, N. Roussel, Properties of fresh and hardened concrete, Cem. Concr. Res. 41 (7) (2011) 775–792.
[2] B. Zhou, Y. Uchida, Influence of flowability, casting time and formwork geometry on fiber orientation and mechanical properties of UHPFRC, Cem. Concr. Res. 95 (2017) 164–177.
[3] M.A. Baril, L. Sorelli, J. Réthoré, F. Baby, F. Toutlemonde, L. Ferrara, S. Bernardi, M. Fafard, Effect of casting flow defects on the crack propagation in UHPFRC thin slabs by means of stereovision Digital Image Correlation, Constr. Build. Mater. 129 (2016) 182–192.
[4] Y. Cai, Q.F. Liu, Stability of fresh concrete and its effect on late-age durability of reinforced concrete: An overview, J. Build. Eng. 79 (2023) 107701.
[5] Y. Cai, W. Zhang, C. Yang, R. François, L. Yu, M. Chen, H. Chen, H. Yang, Evaluating the chloride permeability of steel–concrete interface based on concretes of different stability, Struct. Concr. 22 (5) (2021) 2636–2649.
[6] Y. Cai, Q.F. Liu, Numerical investigation on aggregate settlement and its effect on the durability of hardened concrete, in: Proceedings of the 7th International Conference on Durability of Concrete Structures, Jinan, China, 2022.
[7] Y. Cai, Q. Liu, Research progress on the stability of concrete mixtures and its influence on the durability of engineering structures, J. Xi'an Univ. Arch. Tech. 55 (4) (2023) 492–503.
[8] G.H. Tattersall, The rationale of a two-point workability test, Mag. Concr. Res. 25 (84) (1973) 169–172.
[9] Y. Liu, C. Shi, D. Jiao, X. An, Rheological properties, models and measurements for fresh cementitious materials – A short review, J. Chin. Ceram. Soc. 45 (5) (2017) 708–716.
[10] M. Gesoglu, E. Güneyisi, T. Ozturan, H.O. Oz, D.S. Asaad, Shear thickening intensity of self-compacting concretes containing rounded lightweight aggregates, Constr. Build. Mater. 79 (2015) 40–47.
[11] L. Yang, H. Wang, A. Wu, H. Li, A.B. Tchamba, T.A. Bier, Shear thinning and thickening of cemented paste backfill, Appl. Rheol. 29 (2019) 80–93.
[12] D. Jiao, C. Shi, Q. Yuan, Time-dependent rheological behavior of cementitious paste under continuous shear mixing, Constr. Build. Mater. 226 (2019) 591–600.
[13] B. Zhaidarbek, A. Tleubek, G. Berdibek, Y. Wang, Analytical predictions of concrete pumping: Extending the Khatib–Khayat model to Herschel–Bulkley and modified Bingham fluids, Cem. Concr. Res. 163 (2023) 107035.
[14] K. Ma, J. Feng, G. Long, Y. Xie, Effects of mineral admixtures on shear thickening of cement paste, Constr. Build. Mater. 126 (2016) 609–616.
[15] D. Feys, R. Verhoeven, G.D. Schutter, Why is fresh self-compacting concrete shear thickening? Cem. Concr. Res. 39 (6) (2009) 510–523.
[16] B. Yahyaei, G. Asadollahfardi, A.M. Salehi, N. Esmaeili, Study of shear-thickening and shear-thinning behavior in rheology of self-compacting concrete with micro-nano bubble, Struct. Concr. 23 (3) (2022) 1920–1932.
[17] J.J. Assaad, Correlating thixotropy of self-consolidating concrete to stability, formwork pressure, and multilayer casting, J. Mater. Civ. Eng. 28 (10) (2016) 04016107.
[18] F. De Larrard, C.F. Ferraris, T. Sedran, Fresh concrete: A Herschel–Bulkley material, Mater. Struct. 31 (211) (1998) 494–498.
[19] O.H. Wallevik, D. Feys, J.E. Wallevik, K.H. Khayat, Avoiding inaccurate interpretations of rheological measurements for cement-based materials, Cem. Concr. Res. 78 (2015) 100–109.
[20] A. Yahia, K.H. Khayat, Analytical models for estimating yield stress of high-performance pseudoplastic grout, Cem. Concr. Res. 31 (5) (2001) 731–738.
[21] K. Vance, G. Sant, N. Neithalath, The rheology of cementitious suspensions: A closer look at experimental parameters and property determination using common rheological models, Cem. Concr. Compos. 59 (2015) 38–48.
[22] I.C. Yeh, Modeling slump flow of concrete using second-order regressions and artificial neural networks, Cem. Concr. Compos. 29 (6) (2007) 474–480.
[23] L. Yang, X. An, S. Du, Estimating workability of concrete with different strength grades based on deep learning, Measurement 186 (2021) 110073.
[24] Y. Cai, Q.F. Liu, L. Yu, Z. Meng, Z. Hu, Q. Yuan, B. Šavija, An experimental and numerical investigation of coarse aggregate settlement in fresh concrete under vibration, Cem. Concr. Compos. 122 (2021) 104153.
[25] Y. Cai, Q.F. Liu, Z. Meng, M. Chen, W. Li, B. Šavija, Influence of coarse aggregate settlement induced by vibration on long-term chloride transport in concrete: A numerical study, Mater. Struct. 55 (2022) 235.
[26] Q.F. Liu, X.H. Shen, B. Šavija, Z. Meng, D.C.W. Tsang, S. Sepasgozar, E. Schlangen, Numerical study of interactive ingress of calcium leaching, chloride transport and multi-ions coupling in concrete, Cem. Concr. Res. 165 (2023) 107072.
[27] Q.F. Liu, Y. Cai, H. Peng, Z. Meng, S. Mundra, A. Castel, A numerical study on chloride transport in alkali-activated fly ash/slag concretes, Cem. Concr. Res. 166 (2023) 107094.
[28] L.Y. Tong, Q.X. Xiong, Z. Zhang, X. Chen, G. Ye, Q.F. Liu, A novel lattice model to predict chloride diffusion coefficient of unsaturated cementitious materials based on multi-typed pore structure characteristics, Cem. Concr. Res. 176 (2024) 107351.
[29] L.Y. Tong, Y. Cai, Q.F. Liu, Carbonation modelling of hardened cementitious materials considering pore structure characteristics: A review, J. Build. Eng. 96 (2024) 110547.
[30] C. Karakurt, A.O. Çelik, C. Yilmazer, V. Kiriççi, E. Özyasar, CFD simulations of self-compacting concrete with discrete phase modeling, Constr. Build. Mater. 186 (2018) 20–30.
[31] M. Hosseinpoor, A. Yahia, K.H. Khayat, Modeling of flow performance of self-consolidating concrete using Dam Break Theory and computational fluid dynamics, Cem. Concr. Compos. 102 (2019) 14–27.
[32] W. Cui, J.Y. Zhang, R.C. Miao, H.F. Song, CFD simulation of movement of fresh concrete in the chute during transporting, Constr. Build. Mater. 409 (2023) 134041.
[33] Y. Cai, M. Chen, J. Xia, X.Y. Zhao, G. Prateek, Q. Wang, Q.F. Liu, Numerical modelling of flow performance of fresh concrete considering rheological characteristics, Cem. Concr. Compos. 152 (2024) 105632.
[34] K. Vasilic, B. Meng, H.C. Kühne, N. Roussel, Flow of fresh concrete through steel bars: A porous medium analogy, Cem. Concr. Res. 41 (5) (2011) 496–503.
[35] R. Sassi, A. Jelidi, S. Montassar, Numerical simulation of fresh concrete flow in the L-box test using computational fluid dynamics, Mag. Concr. Res. 75 (23) (2023) 1189–1201.
[36] M. Choi, N. Roussel, Y. Kim, J. Kim, Lubrication layer properties during concrete pumping, Cem. Concr. Res. 45 (2013) 69–78.
[37] R. Comminal, W.R. Leal da Silva, T.J. Andersen, H. Stang, J. Spangenberg, Modelling of 3D concrete printing based on computational fluid dynamics, Cem. Concr. Res. 138 (2020) 106256.
[38] Standardization Administration of the People's Republic of China, GB/T 1346-2011: Test methods for water requirement of normal consistency, setting time and soundness of the Portland cement, 2011.
[39] D. Jiao, C. Shi, Q. Yuan, X. An, Y. Liu, H. Li, Effect of constituents on rheological properties of fresh concrete-a review, Cem. Concr. Compos. 83 (2017) 146–159.
[40] W. Meng, A. Kumar, K.H. Khayat, Effect of silica fume and slump-retaining polycarboxylate-based dispersant on the development of properties of portland cement paste, Cem. Concr. Compos. 99 (2019) 181–190.
[41] D. Kong, D.J. Corr, P. Hou, Y. Yang, S.P. Shah, Influence of colloidal silica sol on fresh properties of cement paste as compared to nano-silica powder with agglomerates in micron-scale, Cem. Concr. Compos. 63 (2015) 30–41.
[42] Standardization Administration of the People's Republic of China, GB/T 50080-2016: Standard for test method of performance on ordinary fresh concrete, 2016.
[43] American Society for Testing and Materials, ASTM C143/C143M-20: Standard test method for slump of hydraulic-cement concrete, 2020.
[44] W.R. Schowalter, G. Christensen, Toward a rationalization of the slump test for fresh concrete: Comparisons of calculations and experiments, J. Rheol. 42 (4) (1998) 865–870.
[45] S. Clayton, T.G. Grice, D.V. Boger, Analysis of the slump test for on-site yield stress measurement of mineral suspensions, Int. J. Miner. Process. 70 (2003) 3–21.
[46] A.G. Darbyshire, T. Mullin, Transition to turbulence in constant-mass-flux pipe flow, J. Fluid Mech. 289 (1995) 83–114.
[47] K.V. Sharp, R.J. Adrian, Transition from laminar to turbulent flow in liquid filled microtubes, Exp. Fluids 36 (5) (2004) 741–747.
[48] T.C. Papanastasiou, Flows of materials with yield, J. Rheol. 31 (5) (1987) 385–404.
[49] A.N. Alexandrou, T.M. McGilvreay, G. Burgos, Steady Herschel–Bulkley fluid flow in three-dimensional expansions, J. Non-Newton. Fluid Mech. 100 (2001) 77–96.
[50] W. Wu, X. Huang, H. Yuan, F. Xu, J. Ma, A modified lattice boltzmann method for herschel-bulkley fluids, Rheol. Acta 56 (4) (2017) 369–376.
[51] Z. Meng, Y. Zhang, W.K. Chen, C.Q. Fu, Q.X. Xiong, C.L. Zhang, Q.F. Liu, A numerical study of moisture and ionic transport in unsaturated concrete by considering multi-ions coupling effect, Transp. Porous Med. 151 (2) (2024) 339–366.
[52] L.Y. Tong, Q.F. Liu, Q.X. Xiong, Z. Meng, Q. Amiri, M. Zhang, Modelling the chloride transport in concrete from microstructure generation to chloride diffusivity prediction, Comput. Aided Civ. Infrastruct. Eng. (2025), https://doi.org/10.1111/mice.13331.
[53] Y. Cai, Q.F. Liu, Numerical estimation on chloride erosion resistance of alkali-activated concrete, J. Build. Mater. 26 (6) (2023) 596–603. +622.
[54] L.Y. Tong, B. Šavija, M. Zhang, Q.X. Xiong, Q.F. Liu, Chloride penetration in concrete under varying humidity and temperature changes: A numerical study, Constr. Build. Mater. 458 (2025) 138380.
[55] X. Gao, Q.F. Liu, Y. Cai, L.Y. Tong, Z. Peng, Q.X. Xiong, G.D. Schutter, A new model for investigating the formation of interfacial transition zone in cement-based materials, Cem. Concr. Res. 187 (2025) 107675.
[56] X. Gao, Z. Peng, L.Y. Tong, Y. Cai, J. Xiao, X. Geng, Q.F. Liu, Effect of global aggregate distribution on interfacial transition zones in cement-based materials: An analytical-numerical study, Constr. Build. Mater. 458 (2025) 138278.
[57] Q.F. Liu, Z. Hu, X.E. Wang, H. Zhao, K. Qian, L.J. Li, Z. Meng, Numerical study on cracking and its effect on chloride transport in concrete subjected to external load, Constr. Build. Mater. 325 (2022) 126797.
[58] Z. Meng, Q.F. Liu, J. Xia, Y. Cai, X. Zhu, Y. Zhou, L. Pel, Mechanical–transport–chemical modeling of electrochemical repair methods for corrosion-induced cracking in marine concrete, Comput. Aided Civ. Infrastruct. Eng. 37 (14) (2022) 1854–1874.
[59] A. Yahia, Effect of solid concentration and shear rate on shear-thickening response of high-performance cement suspensions, Constr. Build. Mater. 53 (2014) 517–521.

[60] D. Feys, J.E. Wallevik, A. Yahia, K.H. Khayat, O.H. Wallevik, Extension of the Reiner–Riwlin equation to determine modified Bingham parameters measured in coaxial cylinders rheometers, Mater. Struct. 46 (1–2) (2013) 289–311.
[61] N. Roussel, Correlation between yield stress and slump: Comparison between numerical simulations and concrete rheometers results, Mater. Struct. 39 (4) (2006) 501–509.
[62] T. Sedran, F.De Larrard, Optimization of Self Compacting Concrete thanks to Packing Model, in: Proceedings of the 1st International RILEM Symposium on Self-Compacting Concrete, Stockholm, Sweden, 1999, pp. 321–332.
[63] A.W. Saak, H.M. Jennings, S.P. Shah, A generalized approach for the determination of yield stress by slump and slump flow, Cem. Concr. Res. 34 (3) (2004) 363–371.
[64] T.Y. Lo, P.W.C. Tang, H.Z. Cui, A. Nadeem, Comparison of workability and mechanical properties of self-compacting lightweight concrete and normal self-compacting concrete, Mater. Res. Innov. 11 (1) (2007) 45–50.
[65] B. Chen, J. Liu, Experimental application of mineral admixtures in lightweight concrete with high strength and workability, Constr. Build. Mater. 22 (6) (2008) 1108–1113.
[66] G. Heirman, R. Hendrickx, L. Vandewalle, D. Van Gemert, D. Feys, G.De Schutter, B. Desmet, J. Vantomme, Integration approach of the Couette inverse problem of powder type self-compacting concrete in a wide-gap concentric cylinder rheometer: Part II. Influence of mineral additions and chemical admixtures on the shear thickening flow behaviour, Cem. Concr. Res. 39 (3) (2009) 171–181.
[67] H. Wu, H. Lei, Y.F. Chen, Grey relational analysis of static tensile properties of structural steel subjected to urban industrial atmospheric corrosion and accelerated corrosion, Constr. Build. Mater. 315 (2022) 125706.
[68] J.C. Du, M.F. Kuo, Grey relational-regression analysis for hot mix asphalt design, Constr. Build. Mater. 25 (5) (2011) 2627–2634.